ADVANCED ENGINEERING MATERIALS
www.aem-journal.com

Optimized Design and Development of a Bioresorbable High Rotational Stability Fixation System for Small Bone Fragments

*Alberto Cingolani, Tommaso Casalini, Marco Riccardo Binelli, Eleonora Cignoli, Lorenza Di Gialluca, Fabio Zambon, Tomaso Villa, Carlo Francesco Grottoli, Kaj Klaue, Filippo Rossi, and Giuseppe Perale**

Bioresorbable pins are experiencing a growing interest and a likewise increasing use in orthopedic surgery for bone fixation. Indeed, such devices are naturally degraded by the human body and a subsequent surgery for their removal is not needed. However, bioresorption has a remarkable side effect on the performance of the devices, since mechanical properties decay over time. This aspect is essential for bone healing. In the first 60 days, the pin must bear continuous mechanical stress while preventing torsional slip of bone fragments. Although torsional support can be improved with suitable pin section design, degradation kinetics and the consequent loss in mechanical stability are slowed down while using high molecular weight polymers, whose slow bioresorption increases recovery time and negatively affects patient care. Herein, a bioresorbable pin of new conception, in terms of cross-sectional shape and material formulation, is presented. Both section and polymer design are optimized through comprehensive mathematical modeling, which synergistically combines degradation and mechanical loads. As a result of the model, bioresorption time is minimized, whereas adequate mechanical resistance is ensured for the first 60 days. The most promising device is then injection molded, sterilized, mechanically tested, and successfully evaluated ex vivo in human femoral heads.

1. Introduction

Osteosynthesis is a common practice for treating fractures. The alignment of bone fragments is essential for achieving normal function after bone healing, which occurs either by direct (without callus) or by indirect (with callus) means.[1] Broadly, two adjacent bone segments can be held together with the help of an internal fixation device. A major option, in this respect, is represented by Kirschner wires.[2] Composed of metal, they can be inserted within the body of the patient and properly tailored in size and length to ensure appropriate fixation. In general, they have diameters of 0.8 or 2.5 mm and are removed after about 3–8 weeks. Even if their clinical efficacy is demonstrated,[2–5] they can be a source of different complications. For instance, if the wire crosses the skin during healing, there is a high likelihood for infection. Moreover, if the pin lies beneath the

Dr. A. Cingolani, C. F. Grottoli, Prof. G. Perale
Industrie Biomediche Insubri IBI SA
Via Cantonale 67, Mezzovico-Vira 6805, Switzerland
E-mail: giuseppe.perale@usi.ch

Dr. T. Casalini
Department of Chemistry and Applied Bioscience
Institute for Chemical and Bioengineering
ETH Zurich
Vladimir-Prelog-Weg 1-5/10, Zürich 8093, Switzerland

Dr. T. Casalini, Prof. G. Perale
Polymer Engineering Laboratory
Institute for Mechanical Engineering and Materials Technology
University of Applied Sciences and Arts of Southern Switzerland (SUPSI)
Via Cantonale 2C, Galleria 2, Manno 6928, Switzerland

M. R. Binelli
Department of Materials
ETH Zurich
Vladimir-Prelog-Weg 1-5/10, Zürich 8093, Switzerland

The ORCID identification number(s) for the author(s) of this article can be found under https://doi.org/10.1002/adem.201901505.

DOI: 10.1002/adem.201901505

E. Cignoli, F. Zambon, Prof. T. Villa, Prof. F. Rossi
Department of Chemistry, Materials and Chemical Engineering "G. Natta"
Politecnico di Milano
Milan 20133, Italy

L. Di Gialluca
DIMEAS
Politecnico di Torino
Torino 10129, Italy

Dr. K. Klaue
Clinica Luganese Moncucco
Via Moncucco 10, Lugano 6900, Switzerland

Prof. G. Perale
Faculty of Biomedical Sciences
Università della Svizzera Italiana (USI)
Via G. Buffi 13, Lugano 6900, Switzerland

Prof. G. Perale
Ludwig Boltzmann Institute for Experimental and Clinical Traumatology
Donaueschingenstrasse 13, Vienna 1200, Austria

skin and close to the bone or buried within the deep tissue, removal may result in a major surgical intervention.[6] In contrast, bioresorbable fixation devices offer a less aggressive alternative[7,8] to hold together small bone fragments such as those found in human phalanges. As discussed by Nielson et al.,[9] internal fixation is needed for a time span that ranges from 4 to 8 weeks, where bony union is formed; after this phase, the internal fixation is no longer required. Therefore, the use of bioresorbable fixation pins coupled with properly tuned degradation kinetics would provide two main advantages: optimizing bone healing and avoiding the need of a second surgical intervention for pin removal, which is instead degraded in situ.

Starting from the pioneering work of Rokkanen et al.[10] in 90s, it is estimated that thousands of surgical interventions using bioresorbable pins are performed worldwide every year covering all aspects of orthopedic casuistry. Aliphatic polyesters, mostly the homopolymer of pure L-lactic acid (PLLA), or its copolymers combining both D- and L-enantiomeric forms (poly(DL)-lactic acid [PDLLA]), glycolic acid (PLGA), and ε-caprolactone (poly(L)-lactide-*co*-ε-caprolactone [PLACL]), have become an established choice for the production of resorbable devices because they degrade by hydrolysis-forming products which are recognized and metabolized by the body itself.[11,12] Because of these features, starting from the 80s, many researchers have spent considerable effort in the study and characterization of such polyesters, resulting in the current comprehensive knowledge of the degradation mechanisms as well as the main factors affecting degradation kinetics, namely, molecular weight and polymer composition.[13] Chain scission occurs through hydrolysis and it is possible to identify two different degradation regimes according to the relative dynamics of water diffusion in the polymer matrix and water consumption. If hydrolysis reaction is much faster than water penetration, degradation takes place only on a thin layer located at device surface (heterogenous degradation), whereas the bulk remains unaffected. The shape of the device does not change during degradation, but its volume decreases. If water diffusion is faster than its consumption, bulk or homogeneous degradation occurs: the entire volume of the device is subjected to degradation, but it remains constant in time. In general, a geometrical parameter, named critical thickness,[14] can be used to discriminate between the two regimes.

Every chain scission event creates an additional carboxyl terminal that can dissociate, thus lowering the microenvironmental pH (μpH); this leads to an autocatalytic behavior because hydrolysis is enhanced in acidic environments. Finally, hydrolysis of the polymers has a detrimental effect on the mechanical properties of the implanted materials over time. As shown in literature,[15] after degradation, the onset Young modulus does not appreciably change until a threshold molecular weight (M_w) value is reached; at this point, it sharply decreases as molecular weight does, decreasing the mechanical performance. In general, M_w must be larger than 45 kDa to avoid this sudden drop.[15]

This aspect cannot be underestimated, because mechanical resistance plays a key role in the functionality of the device. In service, the pin is continuously subjected to compressive and torsional stress caused by segments weight, musculotendonal tension, and mutual rotation of bone fragments. Therefore, if hydrolysis kinetics is too fast, the pin does not ensure the required stability over the desired time span, negatively affecting bone healing or even impairing it. This problem has been mostly addressed by working with arbitrarily high molecular weight polymers, i.e., with a very slow degradation kinetics.[12] Although effective, this approach considerably increases the time needed for a complete pin resorption (which largely exceeds the time span required to assure bony union), impairing the postsurgical recovery of the patients.

To optimize the balance between suitable bioresorption times and adequate mechanical properties, the engineering of bioresorbable pins must be focused on the cross-sectional shape and the polymer of choice.[16,17] Indeed, a simple circular cross-sectional area does not offer an adequate support for preventing mutual torsional slip. Polygonal cross-sections[18] or grooved surfaces[19] can be used to hinder rotation and are solutions already implemented in some commercial products, although not optimally.

In parallel, the initial molecular weight and composition of the polymer must be tuned as they both affect degradation rate and mechanical properties. An optimal formulation would allow the polymer to dissolve away in synchronicity with the formation of new bone.[20] Finally, the two aforementioned aspects mutually influence each other, which must be considered not to cancel out the benefits of the optimization of each of them.[21]

In this regard, mathematical modeling can support the optimization procedure due to the quantitative description of the involved phenomena and their synergistic effects. As mentioned, previous studies have shed light on the main aspects behind degradation kinetics. This led to many different and validated modeling frameworks for the hydrolysis of aliphatic polyesters, with different levels of details and complexity.[22] Simulations concerning the interplay between degradation and mechanical loads are essentially focused on bioresorbable stents,[23,24] whereas a comprehensive study on bioresorbable fixation pins has not been realized yet. Indeed, simulations usually deal with stress distribution in metallic fixation screws and external fixation plates.[25,26] They use validated constitutive models for mechanical behavior and avoid the problem of the interplay between stress and degradation.

From an experimental point of view, there are clinical studies that confirm the suitability of bioresorbable pins as valid substitutes of metallic wires.[27,28] Up to the best knowledge of the authors, a systematic quantitative analysis is still absent in scientific literature. In other words, there are no relevant studies that rationally analyze degradation rate and the influence of geometry on mechanical behavior, also for what regards commercially available products.

In this work, we discuss a novel technological answer for the design of bioresorbable pins by proposing an alternative cross-section design with a four-lobed section. Model simulations have been used for in silico device design to identify the best cross-sectional shape/raw material combination that can fulfill the requirements of an optimal pin, assuring suitable mechanical performances for the first 60 days. Such a requirement was chosen as a compromise between an adequate behavior during the healing phase (which, as mentioned, ranges from 4 to 8 weeks) and a maximized degradation kinetics, so that the pin is absorbed as fast as possible.

The optimized polymeric pins have been manufactured by injection molding, sterilized, characterized from a mechanical point of view, and finally tested ex vivo on human femur head.

This study also aims at proposing an engineering approach to rationally optimize bioresorbable fixation pins by quantitatively considering the interplay between material degradation kinetics, mechanical loads, geometry, and their synergistic effects.

2. Results and Discussion

2.1. Pin Optimization and Development

Four copolymers of PLA were selected for the pin optimization phase. All of them are commercially available and certified in medical grade. **Table 1** shows the molecular weight characteristics of those polymers in terms of initial number average molecular weight M_{n_0}, weight average molecular weight M_{w_0}, and polydispersity PD_0. Specifically, P1 and P2 are PLACL, whereas P3 and P4 are PDLLA, respectively. The selection of commercially available materials has been done to ensure the future practical possibility of developing a new medical device. Indeed, visionary research outputs and novel materials often fail to get to the market because of issues related to regulatory compliance. In this respect, the readily available spectrum of feasible, robust, and applicable solutions is still very limited.

The polymers have been cross-simulated with three main geometries, designated as G1, G2, and G3 (**Figure 1**a), derived from the idea of preventing torsional slips within the two connected fragments.[8] All of them present a four-lobed section, around a fixed circular one of a defined diameter of 2 mm. Specifically, geometry 1 (G1) has a rather smooth lobe shape, whereas geometry 3 (G3) has a very sharp one, and geometry 2 (G2) presents an intermediate situation. Finally, the contribution of postprocessing, such as injection molding or terminal sterilization (Figure 1c), which has an effect on the degradation kinetics of the device and its initial properties,[29] has been considered. In general, as visible for polymers P1 and P4, the outcome is a reduction of molecular weight distribution ($M_{w_{is}}$, $M_{n_{is}}$, and PD_{is}) of roughly 30%.

The applied load has been rationalized as shown in Figure 1b according to literature findings.[5,30] In more detail, the pin is fixed on one extremity, whereas a uniform pressure of 2.5 MPa (i.e., the one produced by a body weight of ≈800 N[31]) is applied on the other one. A torque equal to 1 N m is applied on the lobe surfaces that are in direct contact with the bone to reproduce a realistic torsional slip of two small bone segments from a body extremity.

Table 1. Selected polymer formulations for device optimization. Characterization via GPC was initially done for all pristine polymers, whereas GPC after injection molding and sterilization was performed only for those who were identified as suitable for further application (P1 and P4). Due to this, no values for P2 and P3 were collected.

ID	Type	Supplier	M_{w_0} [kDa]	M_{n_0} [kDa]	PD_0 [–]	$M_{w_{is}}$ [kDa]	$M_{n_{is}}$ [kDa]	PD_{is} [–]
P1	Poly(L)-lactide-*co*-ε-caprolactone	Corbion	183	114.4	1.6	119	67	1.79
P2	Poly(L)-lactide-*co*-ε-caprolactone	Evonik	80	65	1.23	–	–	–
P3	Poly(DL)-lactic acid	Corbion	76	40	1.9	–	–	–
P4	Poly(DL)-lactic acid	Corbion	200	140	1.4	140	107.7	1.3

The bioresorbability of aliphatic polyesters is one of their most attractive properties, but it must be carefully accounted for in device development, since the decay of mechanical properties over time is strongly connected to degradation extent.[32–35] In the framework of in silico optimal device design, a comprehensive description of degradation must take into account the synergistic interplay between kinetics and mass transport. Because of this, the modeling framework proposed by Casalini et al.[36,37] was here adopted because of its validated results. The model combines a mechanistic description of the involved phenomena (hydrolysis, autocatalysis, and mass transport) with the computational efficiency provided by the method of the moments. The model needs only one adjustable parameter, that is, degradation kinetic constant, which was estimated for each material from literature data (details are reported in the Supporting Information). Up to the best knowledge of the authors, a constitutive law that links degradation rate and mechanical loads is not available for aliphatic polyesters. To qualitatively account for the effects of the applied loads, an empirical formula that relates the degradation kinetic constant with Von Mises stress was developed and validated from literature data[38] where the effect of mechanical loads on the molecular weight decay rate of PDLLA devices is reported.

The optimization procedure was conducted with a hierarchical approach of increasing complexity, as shown in **Figure 2**. The four polymers and the three geometries have been cross-simulated. Initially, only the degradation kinetic has been considered as a function of the polymer composition and the geometrical shape of the cross-section. This has been done in both sterilized and unsterilized conditions. The polymers that were not rejected were further simulated coupling the chemical model with the mechanical one. This way, the effect of mechanical load on degradation kinetics is quantitatively considered. Finally, promising polymer candidates have been mechanically tested. Again, this acted as a test for final polymer selection: the one that showed insufficient or unsuitable mechanical properties was discarded. The remaining candidate was finally injection molded into final pin design, sterilized, and tested, also on ex vivo samples.

As previously mentioned, pin degradation without applied mechanical loads was initially simulated, to immediately discard those material/shape combinations that would exhibit a too fast molecular weight decay as it is. Simulation outcomes led to two interesting results, shown in **Table 2**, where M_w values after 60 days are reported for every material/geometry combination. First, G3 geometry exhibited a faster degradation rate than G1 and G2 ones for the same material, as shown in **Figure 3**a, reporting molecular weight decay for polymer P4. This can be directly related to cross-sectional shape: G3 geometry has the lowest diffusive path for water penetration in the matrix, which implies a larger water uptake and thus a faster degradation, by virtue of its smaller volume. Second, model results suggested that P2 and P3 polymer were not able to fulfill the requested requirement and could be immediately discarded as potential

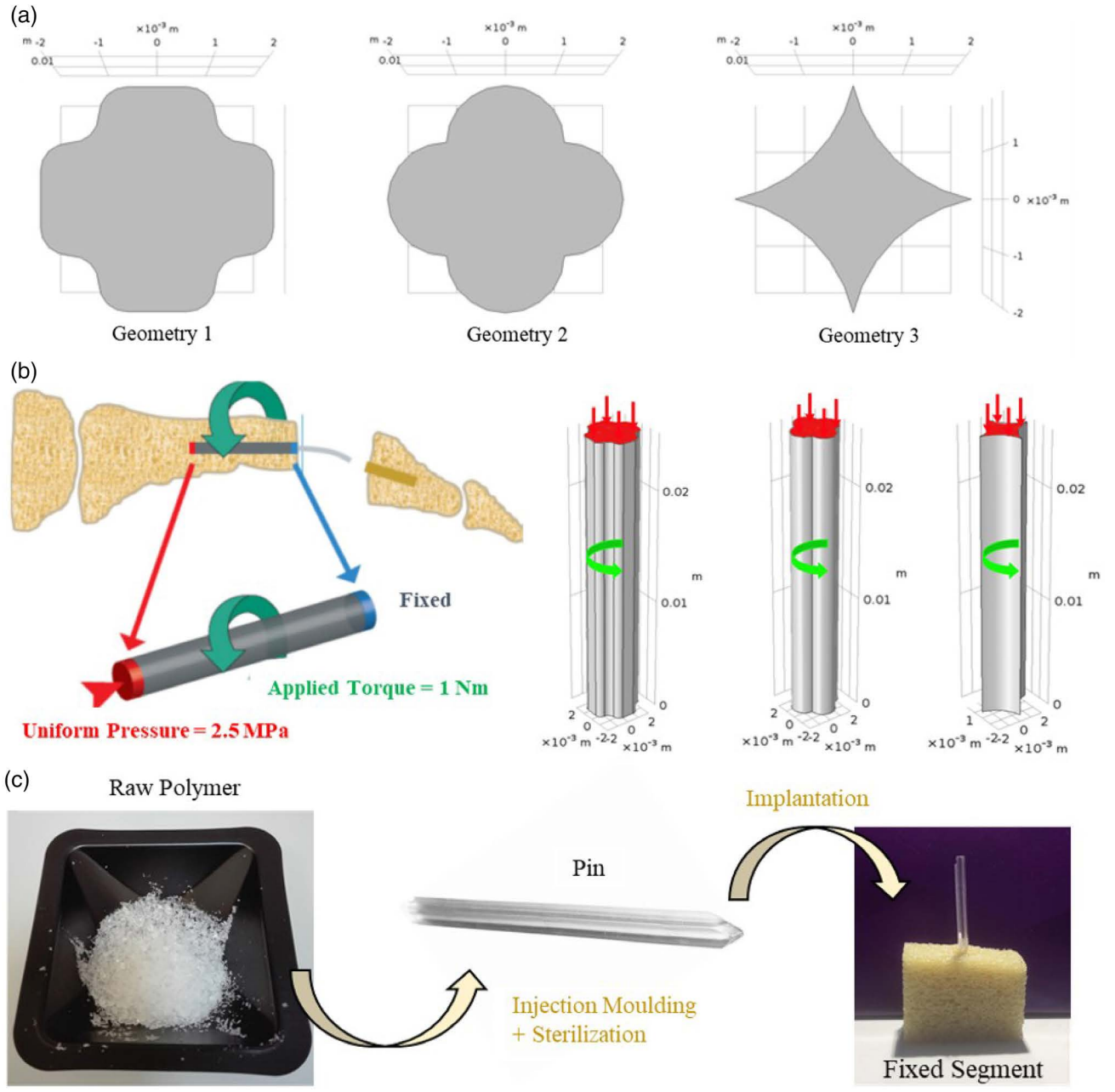

Figure 1. a) Cross-sectional shapes for bone fixation pins proposed and investigated in this work. b) Rationalization of the mechanical load applied to the pin. c) Summary of the here-presented work.

candidates. Therefore, all the subsequent analyses were performed considering only the high molecular weight polymers P1 and P4.

The second phase of the in silico optimization combined the degradation model with a structural mechanics model (assuming a linear elastic material), to evaluate the impact of the mechanical stresses on molecular weight decay and to shed light on stress distribution through the pin; the results are shown in Table 2.

The presence of mechanical stresses accelerates the degradation of the pins of about 20% for G1 and G2 and 50% for G3 (Figure 3b). This is particularly noticeable in the G3/P1 combination, as PLACL has a kinetics constant about five times higher than poly(DL)-lactic acid. Therefore, the local sudden increase in the degradation rate leads to an enhanced production of acidic oligomers, thus to an amplified autocatalytic effect. The main reduction of molecular weight is particularly evident on the lobes, where the maximal stress is present (Figure 3c). The degradation is also not homogeneous over the whole pin body, but it is more relevant on sectors that are closer to the point where load is applied. Moreover, in all cases, G3 exhibits the fastest degradation kinetics. This can be explained by the combined action of load and hydrolysis

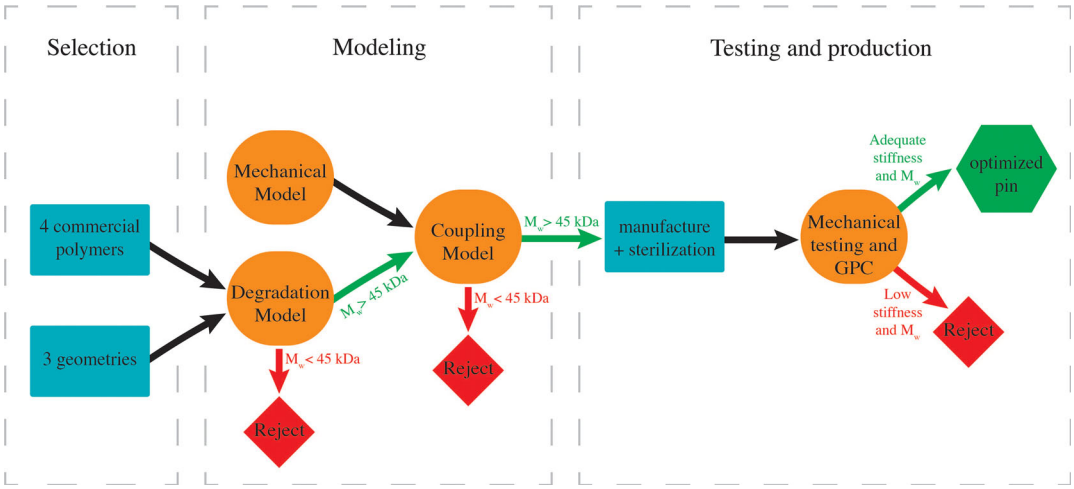

Figure 2. Scheme of the optimization strategy.

Table 2. Weight average molecular weight, expressed in kDa, after 60 days for different geometry/material combinations. In case of polymers P2 and P3, no simulation was performed with applied load as already unloaded conditions presented a too fast degradation.

	M_w [kDa] No load applied (simulated values)				M_w [kDa] Mechanical load applied (simulated values)			
	P1	P2	P3	P4	P1	P2	P3	P4
G1	89.6	40.8	46.4	124.3	80.5	–	–	119.7
G2	86.6	39.6	45.9	123.1	77.3	–	–	118.0
G3	65.9	31.1	41.7	113.0	46.6	–	–	100.1

mechanism. Indeed, the higher the load, mostly concentrated on the external section of the pin's body, the faster is the degradation. In contrast, being able to cope with the minimum required molecular weight within 60 days, practically, G3 resulted to be the best option in terms of cross-section of the device. As a matter of fact, it is the one that opposes the highest resistance to torsional slips, still preserving appropriate mechanical and chemical properties.

Summarizing, model results suggested that G3/P1 and G3/P4 are a feasible geometry/material combination, with the last one being the most promising one. These materials have been mechanically tested, to verify the hypothesis of linear elastic

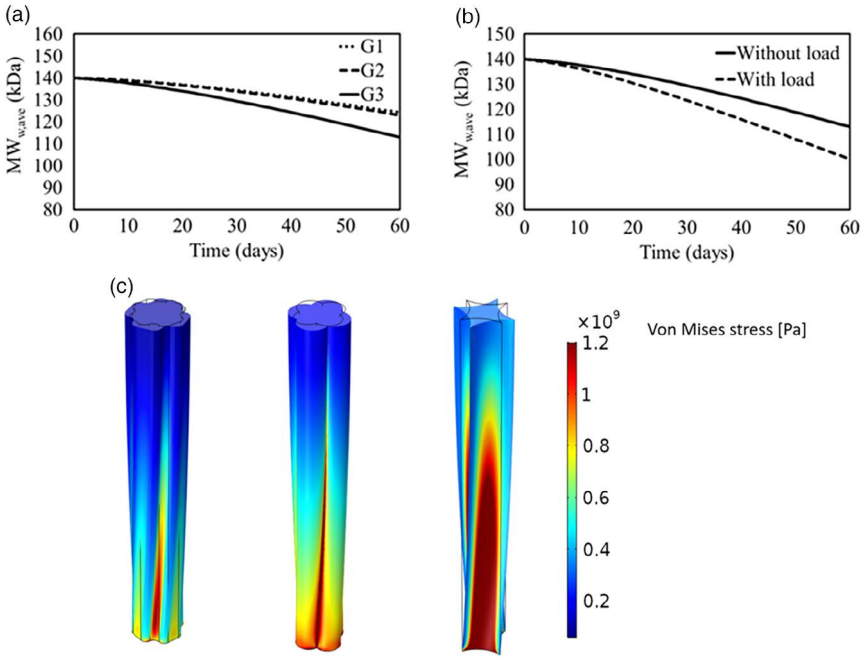

Figure 3. a) Simulated weight average molecular weight as a function of degradation time for P4 polymer. b) Weight average molecular weight as a function of degradation time for G3/P4 combination, without (continuous line) and with (dashed line) applied mechanical load. $M_{w,ave}$ indicates that molecular weight values were averaged over device volume. c) Von Mises stress distribution for P4 polymer and the three investigated geometries.

material used in the calculations and assess their suitability for future clinical application.

2.2. Mechanical Characterization

Tensile, flexural, and torsional testing were performed to properly evaluate the behavior of the pins against the stresses in situ.

Initially, dog-bone samples composed of P1 have been tested for materials selection; the results are shown in **Table 3**. P1 presents a small elastic field (**Figure 4**a), whereas it has a huge plastic deformation prior to failure (Figure 4d). This is not surprising, considering that its composition contains 30% polycaprolactone (in moles), which considerably reduces the brittleness of the fabricated constructs and the stiffness of the polymer itself. This makes the polymer inadequate for an application such as an implantable pin. Indeed, it would not be able to penetrate within the bone segment during insertion, without experiencing excessive deformation or even damage. This way, even though P1 showed a fitting degradation kinetics, only P4 was finally left as a suitable candidate among the ones initially selected, which fulfills the necessity of being certified as applicable for an implantable medical device (expected to be a class III[12]). Thus, molded pins were directly produced and tested in tensile strength, three-point bending and torsion; results are showed in Table 3 and explicative examples are shown in Figure 4. As shown in Figure 4e,f, in case of bending and torsion tests, the pins did not experience failure at the end of machine rotational range, by far higher than any possible physiologic one. Although the stress was enough to compromise the polymer structure, visible by the opaque color at the point of stress application, it was not sufficient to lead to breakage. That is why maximum values for stress and strain have been extracted within the elastic range. Indeed, the pin, when in service, should never reach an irreversible plastic deformation as this would inevitably affect its structural support and impair the overall healing process.

As shown in Table 3, the pins formed using P4 display a stiffness comparable with commercially used PLA grades[39,40] and could be taken into consideration as fitting for the production of an implant. In addition, the measurements performed on P4 display that the material possesses a quite wide linear deformation range, which validates the calculations performed in the model presented here. Finally, it has a quite remarkable resistance to torsion and bending.

2.3. Ex Vivo Testing

The pins, including G3 cross-section measuring about 4.5 mm (outer diameter) and polymer P4, were applied under simulated clinical conditions ex vivo. A fresh, nonrefrigerated explanted femoral head was used, after having been harvested during an independent hip prosthesis surgery and been anonymously donated with informed consent for research purposes. The femoral head was divided into two equivalent halves using an oscillating saw (**Figure 5**a). Reducing the osteotomy using a reduction clamp, both fragments were firmly held together by compression. A helicoidal drill bit was used with an electric drill performing a hole at about right angle to the osteotomy (Figure 5b,c). The pin was implanted using a plunger and a mallet (Figure 5d). The clamp was then removed and the rotational stability between both bony halves was evaluated (Figure 5e), applying force by simple hand twist.

As a matter of fact, there was no possible decoaptation of both bones. Moreover, interfragmentary rotation within the osteotomy plane was noticeable within a magnitude of fractions of a degree up to a maximum of 2°. Macroscopically, it seemed to see four rays penetrating smoothly within the trabeculi of the cancellous bone creating a fully form fit within the femoral head (Figure 5f,g). Once again, this outcome practically validates the selection of the combined cross-section and polymer derived from the results of our approach.

3. Conclusions

In this work, we have developed from conception to actual production an optimized bioresorbable pin for osteosynthesis treatment of small bones. This has been done using a quantitative approach that accounted for degradation kinetics, mechanical stress, geometry, and their synergistic effects. Simulations of different geometries and compositions have been performed, aiming at addressing in one solution two of the main issues found in current commercial products: the lack of rotational stability and the long degradation times. The final optimized design has been produced and extensively tested. As a matter of fact, it could enable optimal degradation time and could ensure prevention of torsional slips and adequate mechanical resistance. Moreover, the pin was easily inserted within human bone, without any damage and perfectly fitting within the surrounding trabeculi. In this respect, this study is a robust proof of concept for an effective industrial product development of the next generation of implantable and bioresorbable osteosynthesis pins.

4. Experimental Section

Model Development: The modeling framework proposed by Casalini et al.[36,37] was adopted here. It had been developed for the simulation

Table 3. Results from mechanical testing. Samples made of P1 (dog bone) have been tested only with tensile tests. Pins produced from P4 have been tested via tensile, torsion, and three-point bending test.

ID	Tensile tests			Torsion tests			Three-point bending		
	Young modulus [GPa]	Max strain [–]	Max stress [MPa]	Shear modulus [GPa]	Max strain [–]	Max stress [MPa]	Young modulus [GPa]	Max strain [–]	Max stress [MPa]
P1	0.280 ± 0.028	2.86 ± 0.27	22.1 ± 0.1	–	–	–	–	–	–
P4	1.1 ± 0.1	0.07 ± 0.01	42.8 ± 3.4	2.6 ± 0.6	0.043 ± 0.013	197 ± 129	3.19 ± 0.02	$0.009 \pm 6.4\,E{-7}$	28.6 ± 0.1

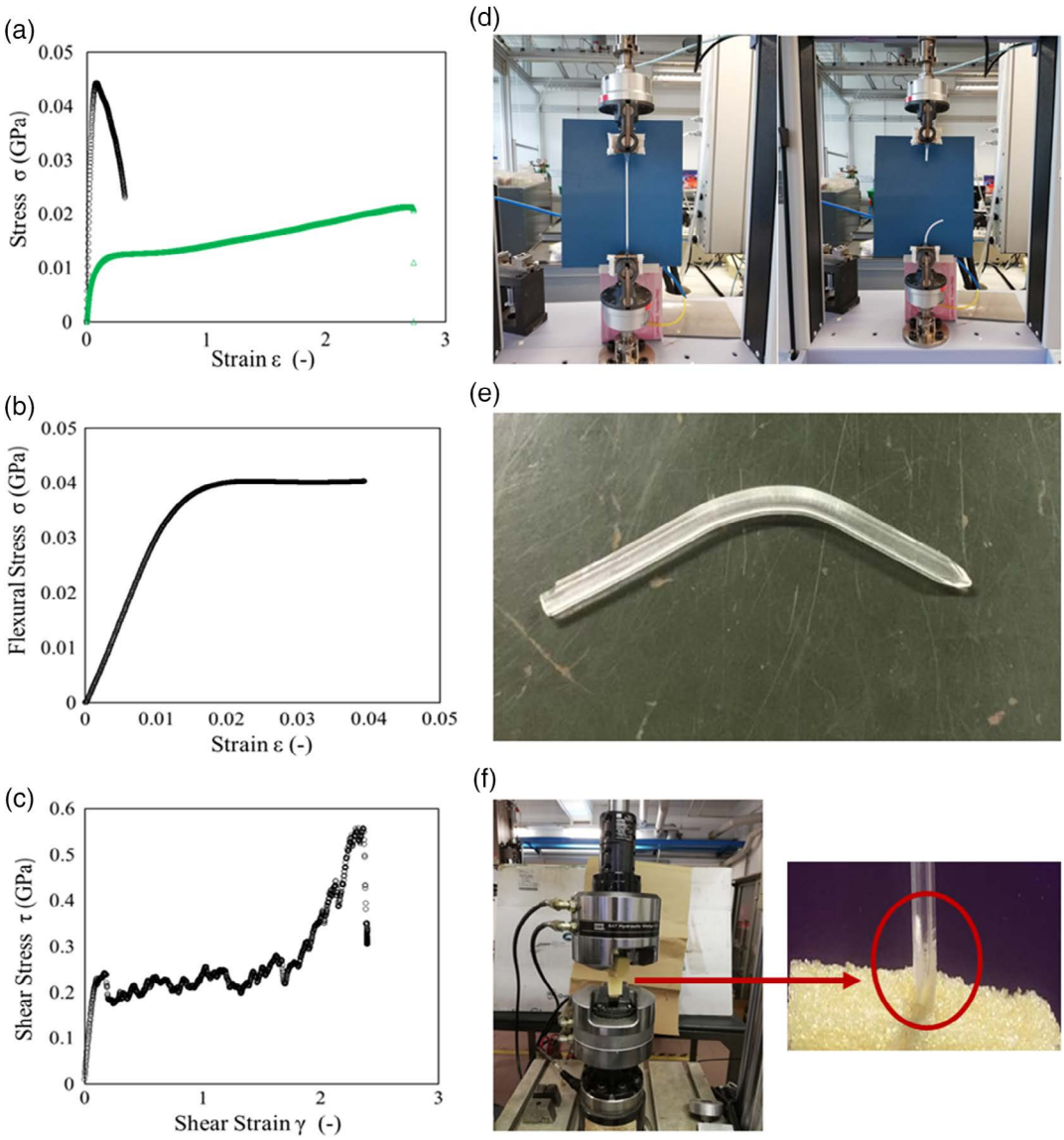

Figure 4. Representative samples out of the mechanical characterization. a) The tensile strength tests for P1 (green triangles) and P4 (black circles); b) the measurement for three-point bending on polymer P4; and c) the torsional tests, always for polymer P4. d) Two moments of the tensile test executed on polymer P1. Specifically, the long elongation before breakage can be observed. e) Pin extracted from bending test machine, unbroken. f) Pins extracted from torsion test machines. As visible, the polymer turned opaque at the point of stress application.

of bulk-eroding polymers and combines a comprehensive description of the involved phenomena (i.e., the effect of autocatalysis and transport phenomena on time- and space-dependent hydrolysis kinetics) and the computational efficiency due to the method of the moment applied to population balances. The overall model was constituted by a system of 13 partial differential equations, related to the temporal and special evolution of monomer (Equation (1)), oligomers up to nonamers (Equation (2)), water (Equation (3)), and the statistical moments of chain length distribution of the first three orders (Equation (4)–(6)).

$$\frac{\partial C_M}{\partial t} = \nabla(D_M \nabla C_M) + 2k_d C_w(\mu_0 - C_M)\mu_0 \tag{1}$$

$$\frac{\partial C_n}{\partial t} = \nabla(D_n \nabla C_n) + 2k_d C_w\left(\mu_0 - \sum_{j=1}^{n} C_j\right)\mu_0 - (n-1)k_d C_w C_n \mu_0 2 \leq n \leq 9 \tag{2}$$

$$\frac{\partial C_w}{\partial t} = \nabla(D_W \nabla C_W) - k_d C_w(\mu_1 - \mu_0)\mu_0 \tag{3}$$

$$\frac{\partial \mu_0}{\partial t} = \sum_{j=1}^{9} \nabla\left(D_j \nabla C_j\right) + k_d C_w(\mu_1 - \mu_0)\mu_0 \tag{4}$$

$$\frac{\partial \mu_1}{\partial t} = \sum_{j=1}^{9} j\nabla\left(D_j \nabla C_j\right) \tag{5}$$

$$\frac{\partial \mu_2}{\partial t} = \sum_{j=1}^{9} j^2 \nabla\left(D_j \nabla C_j\right) + \frac{k_d C_w \mu_0}{3}\left(\mu_1 - 2\frac{\mu_2^2}{\mu_1} + \frac{\mu_2 \mu_1}{\mu_0}\right) \tag{6}$$

The properties of interest can be computed in a straightforward way from statistical moments

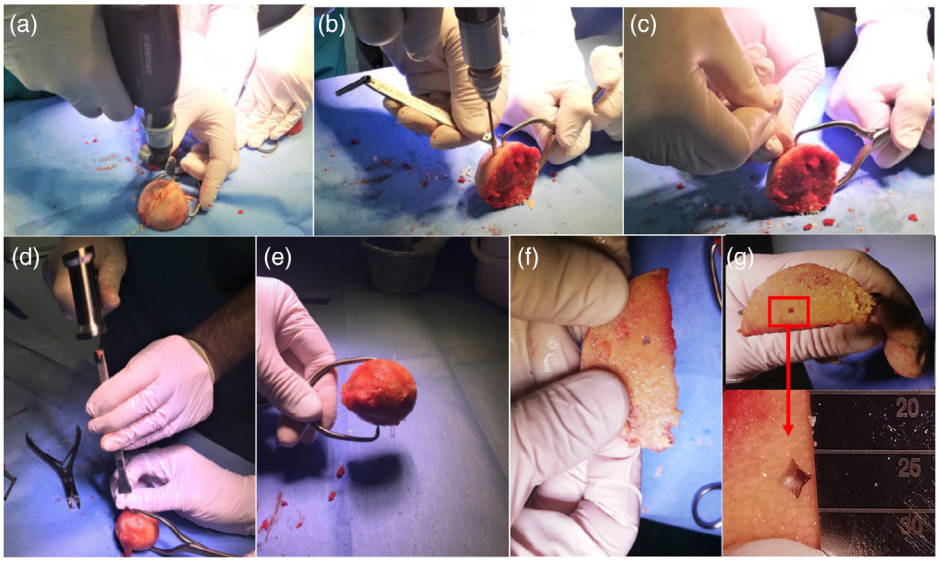

Figure 5. a) Sequence for execution of ex vivo testing on a human femoral head. Initially, the head has been separated in two halves. b) Afterward, a guide hole has been made using a drill and c) the pin put in place. Subsequently, the pin has been d) inserted using a plunger and a mallet, e) holding the two initial halves together. After f) cutting a slice of the bone with the implanted pin inside, g) it is possible to observe that the four rays fully fit within the surrounding bone.

$$M_n = \frac{\mu_1}{\mu_0} MW_{\text{mon}} \tag{7}$$

$$M_w = \frac{\mu_2}{\mu_1} MW_{\text{mon}} \tag{8}$$

$$\text{PD} = \frac{\mu_2 \mu_1}{\mu_1^2} \tag{9}$$

Model derivation, input parameters, boundary conditions, kinetic constant estimation procedure, and the analysis of mesh elements on model outcomes are reported in the Supporting Information.

Pins Production and Processing: Pins were designed using CAD and injection molded accordingly by SamaPlast AG, a plastic processing company in St. Margrethen (Switzerland), under ISO-13485-2016 compliant conditions. The injection molding machine was set to 0.01–1000 g product condition, controlled via microprocessor and applying a 150–3500 kN locking force. In this phase, polymer P4 was supplied as purchased and used without further treatment. The obtained pins had the G3 cross-section appearance, with an internal diameter of 2 mm and a 4 mm outer one, including the limbs. The length of each pin was 59.19 mm.

Terminal sterilization occurred via e-beam irradiation of the samples housed within a carton rack,[41] by Leoni Studer AG (Switzerland), a duly certified sterilization supplier. Electron beam sterilization was applied following a procedure approved and described in the standard ISO 11137. Samples, housed within a carton rack, were passed through the chamber for a few minutes at 47.4 °C and invested by a radiation dose in the range of 25–30 kGy. This way, electrons penetrated the cardboard box and all the samples within the box, ensuring harmful micro-organisms' inactivation. As the electrons penetrate the products, the radiation dose diminishes, with the result that less radiation leaves the box than entered. Thus, boxes were usually turned over and irradiated again from the opposite side for obtaining a relatively uniform dose.

Gel permeation chromatography was used to characterize the polymer pins before and after sterilization. Weight-average (M_w) and number-average molecular weight (M_n) values and molecular weight distribution (M_w/M_n) values were evaluated using a Jasco LC-2000Plus gel permeation chromatograph (GPC) equipped with a refractive index detector RI-2031Plus (Jasco, Oklahoma City, OK, USA) using three Agilent (Santa Clara, CA, USA) PLgel columns, $5 \times 10 - 6$ m particle size, 300×7.5 mm (M_w range: 5×102 to 17×105 g mol^{-1}). Samples were eluted in tetrahydrofuran at a flow rate of 0.5 mL min^{-1} at 35 °C. The GPC samples were injected using a Jasco AS-2055Plus autosampler. The instrument was calibrated using polystyrene standards from 580 to 3 250 000 Da (Polymer Laboratories, Church Stretton, UK). Probes were run in duplicates.

Mechanical Characterization: The tensile, flexural, and torsional properties of the materials and of the constructs investigated in this study were measured under tensile, flexural, and torsional loads. For this purpose, different sets of samples, namely, pins and dog bones, were fabricated. Pins were prepared as described previously. Dog bones, on the other hand, were also injection molded similarly to the pins. The dog bones were 1BA type and had a gauge length of 58 mm thickness of 2 mm and width of 5 mm; the pins were the same as described throughout the study. Sterilized samples were also tested to assess the effect of the sterilization procedure on the mechanical properties of the final parts; a minimum of three samples per conditions were tested.

For tensile and three-point bending tests, a universal mechanical testing machine (Shimadzu AGX, Japan) was used. For tensile testing, the pins were fixed using pressure clamps and secured with epoxy glue for improved stress transfer; dog bones were instead directly clamped on the machine. The strain rate of the test was set to 20 mm min^{-1}. From the data of force and displacement recorded during the test, stress and strain were calculated as follows

$$\sigma = \frac{F}{A} \tag{10}$$

where F is the force applied by the actuator and A is the initial cross-section area, and

$$\varepsilon = \frac{\Delta l}{l_0} \tag{11}$$

where Δl is the vertical displacement recorded during the test and l_0 is the initial length of the specimen. Finally, the elastic modulus ε was calculated as linear regression of the stress–strain curve in the elastic region.

The three-point bending setup in use had a support span of 20 mm, with a crossbar moving at a speed of 20 mm min^{-1}. The test sample is loaded in such a way to create a concave surface at the midpoint with

a specified radius of curvature. From the data of force and displacement recorded during the test, stress and strain were calculated as follows

$$\sigma = \frac{FL/2}{J_F} \times y \tag{12}$$

where F is the applied force, L is the distance between the lower rollers of the bench, J_F is the bending moment of inertia of the specimen, and y is the distance of the section where stress is calculated from the neutral axis, and

$$\varepsilon = \frac{6 \times \Delta l \times y}{L^2} \tag{13}$$

where Δl is the vertical displacement recorded during the test and all the other parameters were already defined. Finally, the elastic modulus ε was again calculated as linear regression of the stress–strain curve in the elastic region.

Torsion tests were run implanting the pins inside blocks of Sawbone of about $40 \times 60 \times 20$ mm. Sawbone (SawBones Europe A/S, Sweden) is a biomechanical test material made of rigid polyurethane foam and used as an alternative to cadaver bone for testing orthopedic implants, instruments, and instrumentation. Specifically, an MTS 858 Bionix servohydraulic testing machine (S/N 1014952, MTS, Minneapolis, MN) was used. The machine was equipped by an axial–torsional hydraulic actuator, with 15 kN axial capacity and 210 Nm torsional capacity, a $\pm$100 mm range LVDT displacement transducer, and a $\pm$140° range ADT angular transducer mounted on the actuator. The load applied to the test sample was measured by an MTS axial/torsional load cell (model 662.20D-04, S/N 1011239, $\pm$15 kN maximum axial load, $\pm$250 Nm maximum torsional load). The machine was driven by a Test Star 790.01 digital controller. The test consisted in holding one of the two Sawbone blocks between the lower jaws of the testing machine and the other between the upper ones, with the pin connecting the two blocks. Tests were run under angle control at a speed of 0.1 deg s^{-1} until a total amount of 140° of rotation was reached. From the data of torque and angle recorded during the test tangential stress and angular strain were calculated as follows

$$\tau = \frac{M_t}{J_T} \tag{14}$$

where M_t is the torque measured by the load cell and J_T is the torsional moment of inertia of the specimen, and

$$\gamma = \frac{\alpha \times r}{l_0} \tag{15}$$

where α is the angle measured during the test, r is the radius of the specimen, and l_0 is the initial length of the specimen. Finally, the tangential modulus G was calculated as linear regression of the tangential stress–strain curve in the elastic region.

Supporting Information

Supporting Information is available from the Wiley Online Library or from the author.

Acknowledgements

A.C. and T.C. contributed equally to this work. This work was partially supported by Swiss InnoSuisse under grant number 34342.1 INNO-LS. The authors thank Prof. André Studart for access to his laboratories.

Conflict of Interest

The authors declare no conflict of interest.

Keywords

biomaterials, bioresorbable polymers, osteosynthesis, small bone fixation

Received: December 8, 2019
Revised: February 13, 2020
Published online:

[1] S. M. Perren, *J. Bone Joint Surg.* **2002**, *84B*, 1093.
[2] B. B. G. M. Franssen, A. H. Schuurman, A. M. Van der Molen, M. Kon, *Acta Orthop. Belg.* **2010**, *76*, 1.
[3] R. M. Jay, D. S. Malay, A. S. Landsman, N. Jennato, J. Huish, M. Younger, *J. Foot Ankle Surg.* **2016**, *55*, 697.
[4] J. Wu, F. Zhou, L. Yang, J. Tan, *Sci. Rep.* **2016**, *6*, 30480.
[5] T. N. Board, L. Yang, M. Saleh, *J. Biomech.* **2007**, *40*, 20.
[6] M. Terndrup, T. Jensen, S. Kring, M. Lindberg-Larsen, *Injury* **2018**, *49*, 1126.
[7] J. A. Planell, *Bone Repair Biomaterials*, Woodhead Publishing Limited, Cambridge **2009**.
[8] W. S. Pietrzak, T. P. Lessek, S. V. Perns, *J. Foot Ankle Surg.* **2006**, *45*, 288.
[9] D. L. Nielson, N. J. Young, C. M. Zelen, *Clin. Podiatr. Med. Surg.* **2013**, *30*, 283.
[10] P. U. Rokkanen, O. Böstman, E. Hirvensalo, E. A. Mäkelä, E. K. Partio, H. Pätiälä, S. Vainionpää, K. Vihtonen, P. Törmälä, *Biomaterials* **2000**, *21*, 2607.
[11] C. K. S. Pillai, C. P. Sharma, *J. Biomater. Appl.* **2010**, *25*, 291.
[12] G. Perale, J. Hilborn, *Bioresorbable Polymers for Biomedical Applications – From Fundamentals to Translational Medicine*, Woodhead Publishing, Cambridge **2016**.
[13] F. Alexis, *Polym. Int.* **2005**, *54*, 36.
[14] F. von Burkersroda, L. Schedl, A. Gopferich, *Biomaterials* **2002**, *23*, 4221.
[15] H. Tsuji, *Polymer* **2002**, *43*, 1789.
[16] R. J. Kroeze, M. N. Helder, L. E. Govaert, T. H. Smit, *Materials* **2009**, *2*, 833.
[17] Z. Sheikh, S. Najeeb, Z. Khurshid, V. Verma, H. Rashid, M. Glogauer, *Materials* **2015**, *8*, 5744.
[18] H. Alexander, N. Langrana, S. B. Massengill, A. B. Weiss, *J. Biomech.* **1981**, *14*, 377.
[19] A. A. Alsheghri, O. Alageel, M. Amine Mezour, B. Sun, S. Yue, F. Tamimi, J. Song, *Acta Biomater.* **2018**, *80*, 425.
[20] X. Zhang, M. F. A. Goosen, U. P. Wyss, D. Pichora, *J. Macromol. Sci. Part C* **1993**, *33*, 81.
[21] M. Prakasam, J. Locs, K. Salma-Ancane, D. Loca, A. Largeteau, L. Berzina-Cimdina, *J. Funct. Biomater.* **2017**, *8*, 44.
[22] T. Casalini, G. Perale, *Durab. Reliab. Med. Polym.* **2012**, *1*, 3.
[23] J. S. Bergström, D. Hayman, *Ann. Biomed. Eng.* **2016**, *44*, 330.
[24] J. S. Soares, J. E. Moore, *Ann. Biomed. Eng.* **2016**, *44*, 560.
[25] M. Nassiri, B. MacDonald, J. M. O'Byrne, *J. Orthop.* **2013**, *10*, 29.
[26] A. R. MacLeod, P. Pankaj, A. H. R. W. Simpson, *J. Biomech.* **2012**, *45*, 1712.
[27] T. B. Hughes, *Clin. Orthop. Relat. Res.* **2006**, *445*, 169.
[28] P. Augat, P. B. Robioneck, A. Abdulazim, F. Wipf, K. S. Lips, V. Alt, R. Schnettler, C. Heiss, *J. Biomed. Mater. Res. Part B* **2016**, *104*, 170.
[29] A. Cingolani, T. Casalini, S. Caimi, A. Klaue, M. Sponchioni, F. Rossi, G. Perale, *Polymers* **2018**, *10*, 851.
[30] I. S. Fyfe, S. Mason, *Hand* **1979**, *11*, 51.
[31] C. Y. Chung, *J. Mech. Behav. Biomed. Mater.* **2018**, *77*, 642.
[32] L. Montanari, F. Cilurzo, L. Valvo, A. Faucitano, A. Buttafava, A. Groppo, I. Genta, B. Conti, *J. Control. Release* **2001**, *75*, 317.
[33] M. C. Gupta, V. G. Deshmukh, *Polymer* **1983**, *24*, 827.

[34] S. C. J. Loo, H. T. Tan, C. P. Ooi, Y. C. F. Boey, *Acta Biomater.* **2006**, *2*, 287.
[35] S. C. J. Loo, C. P. Ooi, Y. C. F. Boey, *Biomaterials* **2005**, *26*, 3809.
[36] T. Casalini, F. Rossi, S. Lazzari, G. Perale, M. Masi, *Mol. Pharm.* **2014**, *11*, 4036.
[37] T. Casalini, F. Rossi, M. Santoro, G. Perale, *Int. J. Mol. Sci.* **2011**, *12*, 3857.
[38] Y. B. Fan, P. Li, L. Zeng, X. J. Huang, *Polym. Degrad. Stab.* **2008**, *93*, 677.
[39] S. Farah, D. G. Anderson, R. Langer, *Adv. Drug Deliv. Rev.* **2016**, *107*, 367.
[40] J. M. Ugartemendia, A. Larrañaga, H. Amestoy, A. Etxeberria, J. R. Sarasua, *Eur. Polym. J.* **2018**, *98*, 411.
[41] N. P. Tipnis, D. J. Burgess, *Int. J. Pharm.* **2018**, *544*, 455.